AIP | Physics of Plasmas

Fast, purely growing collisionless reconnection as an eigenfunction problem related to but not involving linear whistler waves

Paul M. Bellan

Citation: Physics of Plasmas (1994-present) **21**, 102108 (2014); doi: 10.1063/1.4897375
View online: http://dx.doi.org/10.1063/1.4897375
View Table of Contents: http://scitation.aip.org/content/aip/journal/pop/21/10?ver=pdfcov
Published by the AIP Publishing

Fast, purely growing collisionless reconnection as an eigenfunction problem related to but not involving linear whistler waves

Paul M. Bellan
Applied Physics and Materials Science, Caltech, Pasadena, California 91125, USA

(Received 3 August 2014; accepted 23 September 2014; published online 10 October 2014)

If either finite electron inertia or finite resistivity is included in 2D magnetic reconnection, the two-fluid equations become a pair of second-order differential equations coupling the out-of-plane magnetic field and vector potential to each other to form a fourth-order system. The coupling at an X-point is such that out-of-plane even-parity electric and odd-parity magnetic fields feed off each other to produce instability if the scale length on which the equilibrium magnetic field changes is less than the ion skin depth. The instability growth rate is given by an eigenvalue of the fourth-order system determined by boundary and symmetry conditions. The instability is a purely growing mode, not a wave, and has growth rate of the order of the whistler frequency. The spatial profile of both the out-of-plane electric and magnetic eigenfunctions consists of an inner concave region having extent of the order of the electron skin depth, an intermediate convex region having extent of the order of the equilibrium magnetic field scale length, and a concave outer exponentially decaying region. If finite electron inertia and resistivity are not included, the inner concave region does not exist and the coupled pair of equations reduces to a second-order differential equation having non-physical solutions at an X-point. © *2014 AIP Publishing LLC*. [http://dx.doi.org/10.1063/1.4897375]

I. INTRODUCTION

If magnetic reconnection[1–4] did not exist, all magnetized plasmas would forever maintain the same topology as no plasma segment could detach from or merge with another. Observations show that magnetic reconnection frequently occurs in all relevant contexts: laboratory experiments,[5–8] the magnetosphere,[9,10] the solar corona,[11,12] and astrophysics.[13] Observations further indicate that reconnection provides a means for accelerating particles to enormous energies.[14,15]

Magnetic reconnection has traditionally been considered from two somewhat different points of view (cf. historical discussion on pp. 8–9 of Ref. 1 and Chapters 3, 4 of Ref. 16). The first point of view assumes that reconnection is a stationary, steady-state process resulting from some external driving (forcing) mechanism as first discussed by Sweet[17] and by Parker.[18] The second point of view assumes that reconnection is a spontaneous exponentially growing instability; this instability is conventionally called the tearing instability and was first discussed by Furth, Killeen, and Rosenbluth[19] in the context of resistive magnetohydrodynamics (MHD). Steady-state reconnection is characterized by the speed with which incoming plasma approaches the reconnection layer while spontaneous reconnection is characterized by the exponential growth rate. Both the Sweet-Parker and Furth-Killeen-Rosenbluth analyses were done in the context of resistive MHD; a collisionless kinetic tearing instability wherein resonant electron wave-particle absorption in a spatially periodic configuration acted as sink for magnetic energy was proposed by Coppi, Laval, and Pellat.[20]

The stationary and spontaneous points of view can be related to each other by considering steady-state reconnection to be the nonlinear saturated state of an initially exponentially growing instability. This is because in order to achieve steady-state reconnection, a system must evolve through a transient state during which the reconnection grows and this growth would be of the order of the spontaneous growth rate for the given conditions. Thus, if a system started with say a 10% perturbation, the perturbation amplitude would grow to approach the equilibrium amplitude after a couple of exponential growth periods. The instability would then no longer be able to grow according to linear theory in which case the perturbation would become saturated and approximately time-independent.

The induction equation governing magnetic field evolution is obtained by taking the curl of Ohm's law. The generalized Ohm's law is[21]

$$\mathbf{E}+\mathbf{U}\times\mathbf{B}-\underbrace{\frac{\mathbf{J}}{ne}\times\mathbf{B}}_{\text{Hall}}+\underbrace{\frac{\nabla P_e}{ne}}_{\substack{\text{electron}\\ \text{pressure}}}+\underbrace{\frac{m_e}{e}\frac{d\mathbf{u}_e}{dt}}_{\substack{\text{electron}\\ \text{inertia}}}=\underbrace{\eta\mathbf{J}}_{\text{resistive}}. \quad (1)$$

Resistive MHD, the simplest reconnection model, results from dropping Hall, electron inertia, and electron pressure terms from Eq. (1) thereby obtaining $\mathbf{E}+\mathbf{U}\times\mathbf{B}=\eta\mathbf{J}$. The curl of this resistive Ohm's law predicts magnetic reconnection to be a localized, slow η-dependent diffusive process;[1–3,17–19] an estimate of the growth rate of the MHD resistive tearing mode is obtained by postulating that the magnitudes of the three terms in $E_z+\hat{z}\cdot\mathbf{U}\times\mathbf{B}=\eta J_z$ are all of the same order at the reconnection layer. This resistive MHD estimate fails to describe observations in real situations where reconnection typically occurs orders of magnitude faster;[8,10,22–26] fast non-MHD reconnection is also observed in numerical simulations.[27–30]

The simplest approach to studying magnetic reconnection is to consider the temporal evolution of a current sheet,[31] i.e., the two-dimensional situation sketched in Fig. 1. Here, the in-plane equilibrium magnetic field

$B_y = -\partial A_z/\partial x$ reverses direction at $x=0$ and can be modeled as

$$B_y(x) = \bar{B}\tanh(x/L), \tag{2}$$

where L is the current sheet width. This magnetic field has an associated electric current density $J_z = \bar{B}/(\mu_0 L\cosh^2(x/L))$ such that the magnetic force $\mathbf{J}\times\mathbf{B}$ is anti-symmetric with respect to x and directed towards $x=0$. An equilibrium is assumed in which a hydromagnetic pressure P is peaked at $x=0$ so that the gradient of $\partial P/\partial x$ balances the inward magnetic force $-J_z B_y$. Since $P = n\kappa(T_i + T_e)$ the pressure gradient could come from the density gradient if the temperatures T_i, T_e are both uniform, from a T_i or T_e gradient if the density is uniform, or from some combination of density and temperature gradients. For simplicity it will be assumed here that the ion temperature gradient provides the pressure gradient and that both the density n and the electron temperature T_e are spatially uniform. For situations where the temperature is uniform and the density is non-uniform, the model presented here would be approximate because terms of order $n^{-1}dn/dx$ are effectively dropped compared to terms of order $B_y^{-1}dB_y/dx$; such an approximation is reasonable because n would have a maximum near $x=0$ so $n^{-1}dn/dx$ is small near $x=0$ whereas because B_y vanishes near $x=0$, $B_y^{-1}dB_y/dx$ is large near $x=0$.

The hyperbolic behavior (X-point) in Fig. 1 results from adding to A_z a perturbation scaling as $\cos(k_y y)$. The sign of the perturbation is such that in the vicinity of the $y=0$ axis there are inflows in the x direction towards $x=0$ while in the vicinity of the $x=0$ axis there are outflows in the y direction away from $y=0$. At large distance from the X-point these flows are approximately given by $\mathbf{u}_i = \mathbf{u}_e = \mathbf{E}\times\mathbf{B}/B^2$ and so to have the appropriate signs of inflows and outflows, the electric field must be of the form $\mathbf{E} = E_z\hat{z}$ where $E_z > 0$. Since $J_z > 0$, the product $E_z J_z$ is positive implying the reconnection process acts as a sink for electromagnetic energy. In resistive MHD, the plasma resistivity acts as this sink by converting electromagnetic energy into heat (i.e., $E_z J_z = \eta J_z^2$). By contrast, in collisionless reconnection some non-thermal mechanism converts electromagnetic energy into non-random particle energy or else radiates away the electromagnetic energy.

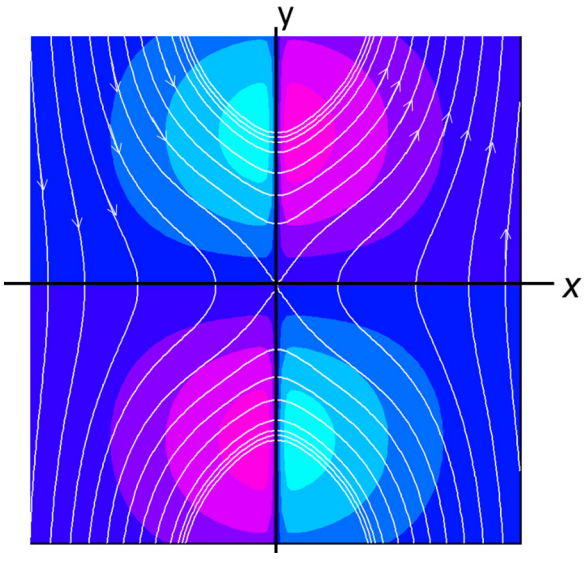

FIG. 1. Sketch of X-point: White lines are contours of constant $A_z(x, y, t)$. The arrows on the white lines show the direction of the in-plane magnetic field $B_T(x, y, t)$ which is up for positive x and down for negative x. The colors show contours of the out-of-plane magnetic field $B_z(x, y, t)$ and shows its quadrupole character. The plot region is $-50 < x, y < 50$. The out-of-plane vector potential is $A_z(x, y) = -\log(\cosh(x/5)) - 5\cos(2\pi y/120)\exp(-(x/30)^2)$ and the out-of-plane magnetic field is $B_z(x, y) = 7\sin(2\pi y/120)\tanh(x/1)\exp(-(x/30)^2)$. A constant offset 2 was added to B_z to make the color tables used antisymmetric; this offset was necessary because of the way the specific color table used maps numbers to colors.

Experimental,[8,24] numerical,[32] and spacecraft[10] observations show that when L becomes smaller than c/ω_{pi}, an out-of-plane quadrupole magnetic field $B_z \sim xy\, g(x^2, y^2)$ appears; here g is some even function of x and of y so B_z is an odd function of x and of y. This quadrupole magnetic field, shown as the red and blue colors in Fig. 1, was first predicted by Sonnerup[33] to be a consequence of the Hall term. Because MHD does not predict the quadrupole magnetic field, its manifestation is considered to signify occurrence of non-MHD Hall processes.

Using numerical simulations of the two-fluid equations, Mandt *et al.*[27] proposed that whistler waves provide the mechanism by which collisionless reconnection is mediated. Rogers *et al.*[28] developed this proposition further and argued that collisionless reconnection is driven by standing whistler waves at the X-point. Fujimoto and Sydora[34] challenged the proposition that whistler waves drive collisionless reconnection because they observed the location of whistler waves in their simulation to be *downstream* of the X-point and *not at* the X-point. Because the whistler waves were not created at the X-point, they argued that whistler waves must be an *effect* of collisionless reconnection rather than a *cause*. The conclusions of Fujimoto and Sydora were supported by Guo *et al.*[35] who observed in their numerical simulation that whistler waves associated with collisionless reconnection were not temporally coincident with the reconnection. Specifically, Guo *et al.* observed that time intervals existed when collisionless reconnection took place but there was no simultaneous evidence of whistler waves.

Using analytic methods, Bulanov *et al.*[36] derived a system of coupled equations retaining finite electron inertia and resistivity. After simplifying these equations by dropping numerous terms, Bulanov *et al.* proposed simple scalings for the simplified equations. Attico *et al.*[37] derived similar systems of equations while Shaikhislamov[38] considered dynamical behavior as L collapsed to the ion and then electron skin depth scale.

We derive and solve fluid equations here that, as in Refs. 27, 28, and 36–38, have Hall terms couple the out-of-plane magnetic field $B_z(x, y, t)$ and the out-of-plane vector potential $A_z(x, y, t)$ to each other. Our approach differs by retaining both electron inertia and resistivity and by solving for the eigenvalues and eigenfunctions of the system of equations. We show that it is essential to include at least one of finite electron inertia or finite resistivity in order for the problem to have physically sensible solutions. From a mathematical point of view, retention of at least one of electron inertia or resistivity provides a fourth order system that has

mathematically regular solutions at $x=0$, whereas dropping both electron inertia and resistivity causes the system to be second order with no regular solutions at $x=0$.

This paper is organized a follows: Section II derives the fourth-order system and shows how it is related to whistler waves. Section III solves the fourth-order system of equations using a two-point boundary value method[39] together with the imposition of certain symmetry and anti-symmetry properties. Section IV presents quantitative comparisons to Magnetic Reconnection Experiment (MRX) measurements.[25,40] Section V shows how omitting both electron inertia and resistivity leads to a second-order differential equation having non-physical solutions at $x=0$. Section VI shows that the eigenvalue of the fourth-order system predicts growth rates in good agreement with the hybrid simulation collisionless growth time reported by Mandt *et al.*[27] Section VII presents conclusions.

II. DERIVATION OF FOURTH-ORDER SYSTEM COUPLING A_z AND B_z

We consider magnetic reconnection for a conventional 2-D Harris[31] current sheet as given in Eq. (2). Scaling arguments[1,38] of the induction equation obtained from the curl of Eq. (1) show that the Hall term becomes important when L is smaller than the ion skin depth c/ω_{pi} and the electron-ion collision frequency ν_{ei} is much smaller than the electron cyclotron frequency ω_{ce}. The electron inertia term scales as c/ω_{pe} and thus is much smaller than the Hall term which scales as c/ω_{pi}. Nevertheless, electron inertia must be retained because, unlike the Hall term, electron inertia can balance the component of $\mathbf{E}$ parallel to $\mathbf{B}$. Ion motion becomes unimportant when $L \le c/\omega_{pi}$ in which case the electric current density $\mathbf{J}$ comes from electron motion only. Thus, one can set $\mathbf{U}=0$ in Eq. (1) when considering dynamics having spatial scale $L < c/\omega_{pi}$. Quasi-neutrality then requires electron motion to be incompressible because ions cannot move to neutralize any spatially non-uniform electron charge concentration.

Making these assumptions and writing $\mathbf{J}=-ne\mathbf{u}_e$, where $\mathbf{u}_e$ is the electron fluid velocity, Eq. (1) reduces to

$$\eta\mathbf{J}+\frac{c^2}{\omega_{pe}^2}\mu_0\left(\frac{\partial\mathbf{J}}{\partial t}-\frac{\mathbf{J}}{ne}\cdot\nabla\mathbf{J}\right)=\mathbf{E}-\frac{\mathbf{J}}{ne}\times\mathbf{B}+\frac{\nabla P_e}{ne}. \quad (3)$$

The out-of-plane and ignorable z direction will be referred to as the axial direction and the directions orthogonal to z as the transverse direction. Because $\partial/\partial z=0$, $E_z=-\partial A_z/\partial t$ and the transverse gradient operator is identical to the full gradient operator, i.e., $\nabla_T=\nabla$. The magnetic field is decomposed into axial and transverse components $\mathbf{B}=B_z\hat{z}+\mathbf{B}_T$ where the transverse component is $\mathbf{B}_T=\nabla A_z\times\hat{z}$. The magnetic field is thus completely determined by the two scalars A_z and B_z. Using Ampere's law, the current density J is decomposed into $\mathbf{J}_T=\mu_0^{-1}\nabla_T B_z\times\hat{z}$ and $J_z=-\mu_0^{-1}\nabla_T^2 A_z$ so $\mathbf{J}$ is also completely determined by A_z and B_z. It is seen that A_z and B_z are the respective stream functions for $\mathbf{B}_T$ and $\mathbf{J}_T$.

Decomposition of Eq. (3) into axial and transverse components gives

$$\eta J_z+\frac{c^2}{\omega_{pe}^2}\mu_0\left(\frac{\partial J_z}{\partial t}-\frac{\mathbf{J}_T}{ne}\cdot\nabla J_z\right)=E_z-\frac{1}{ne}\hat{z}\cdot\mathbf{J}_T\times\mathbf{B}_T, \quad (4a)$$

$$\eta\mathbf{J}_T+\frac{c^2}{\omega_{pe}^2}\mu_0\left(\frac{\partial\mathbf{J}_T}{\partial t}-\frac{\mathbf{J}_T}{ne}\cdot\nabla\mathbf{J}_T\right)=\mathbf{E}_T-\frac{1}{ne}(\mathbf{J}\times\mathbf{B})_T+\frac{\nabla_T P_e}{ne}. \quad (4b)$$

The curl of Eq. (4b) is in the axial direction and, using Faraday's law, is

$$\frac{c^2}{\omega_{pe}^2}\left[\left(\nu_{ei}+\frac{\partial}{\partial t}\right)\nabla_T^2 B_z+\frac{1}{ne}\hat{z}\cdot\nabla_T\times(\mathbf{J}_T\cdot\nabla\mathbf{J}_T)\right]=\frac{\partial B_z}{\partial t}+\frac{1}{ne}\hat{z}\cdot\nabla_T\times(\mathbf{J}\times\mathbf{B})_T, \quad (5)$$

where $\nabla_T\times\mathbf{J}_T=-\hat{z}\mu_0^{-1}\nabla_T^2 B_z$ and $\eta/\mu_0=\nu_{ei}c^2/\omega_{pe}^2$ have been used with ν_{ei} the electron- ion collision frequency. The factor c^2/ω_{pe}^2 appearing in Eqs. (4a) and (5) is proportional to m_e. Because of the assumed exponential time dependence $\exp(\gamma t)$, the inclusion of collisions can thus be considered to be a modification of m_e since adding collisions is equivalent to replacing m_e by $m_e(1+\nu_{ei}/\gamma)$; this is essentially the same as the method by which collisions are added to a wave model (see p. 38 of Ref. 41). Taking the curl of Eq. (4b) annihilated the electron pressure term; this annihilation results from the presumption that the pressure is both isotropic and barotropic. Situations where the pressure is not isotropic or not barotropic are known to introduce additional behaviors and instabilities, but it will be seen here that an extremely fast instability results which does not depend on pressure having these more complicated properties. If the equilibrium density were to be non-uniform then taking the curl of Eq. (4b) would introduce terms depending on the density gradient, but these terms should be of lesser importance than the effect of the magnetic field gradient because the magnetic field goes through zero at $x=0$, whereas the density would be peaked at $x=0$.

At an X-point A_z can be represented as an even function of x with a periodic dependence in the y direction (see Fig. 1). On the other hand, the quadrupole magnetic field associated with Hall reconnection has an odd dependence on x and on y.[33] Consistent with these symmetry properties, we postulate a perturbation expansion $A_z=A_{z0}(x)+\tilde{A}_z(x,y,t)$ and $B_z=\tilde{B}_z(x,y,t)$ where

$$\tilde{A}_z(x,y,t)=e^{\gamma t}a(x)\cos k_y y, \quad (6a)$$

$$\tilde{B}_z(x,y,t)=e^{\gamma t}b(x)\sin k_y y, \quad (6b)$$

and $a(-x)=a(x)$, $b(-x)=-b(x)$. Thus, $\tilde{A}_z$ has the appropriate hyperbolic symmetry of an X-point, while $\tilde{B}_z$ has the desired quadrupole dependence.

We linearize Eqs. (4a) and (5) and define $\varepsilon=c/(\omega_{pe}L)$, $v_{Ae}=\bar{B}/\sqrt{\mu_0 n m_e}$, and the mass-independent, whistler-like frequency $\omega_{wh}=k_y\varepsilon v_{Ae}=k_y L^{-1}\bar{B}/(ne\mu_0)$. On introducing the normalized quantities

$$\xi=x\omega_{pe}/c,\quad \kappa=2^{1/2}\omega_{wh}/\gamma, \quad (7a)$$

$$\bar{k}_y=k_y c/\omega_{pe},\quad \bar{\nu}_{ei}=2^{-1/2}\nu_{ei}/\omega_{wh}, \quad (7b)$$

and defining

$$s = 2^{-1/2} bL, \tag{8}$$

Eqs. (4a) and (5) can be written as

$$(1+\kappa\bar{\nu}_{ei})\left(s'' - \bar{k}_y^2 s\right) - s = \kappa\left(\frac{a'' - \bar{k}_y^2 a}{2\varepsilon^2} + a\left(1 - \tanh^2(\varepsilon\xi)\right)\right)\tanh(\varepsilon\xi), \tag{9a}$$

$$(1+\kappa\bar{\nu}_{ei})(a'' - \bar{k}_y^2 a) - a = \kappa s \tanh(\varepsilon\xi), \tag{9b}$$

where a prime denotes $d/d\xi$ and each term has the dimensions of a vector potential. Equations (9) correspond to Eqs. (9) and (10) in Ref. 37 and in the limit $\varepsilon\xi \ll 1$, Eqs. (9) reduce to Eqs. (32) and (33) of Bulanov *et al.*[36] In the opposite limit where $\varepsilon\xi \to \infty$ and assuming $\bar{\nu}_{ei} = 0$, Eqs. (9) reduce to

$$s'' - \bar{k}_y^2 s - s = \kappa\left(\frac{a'' - \bar{k}_y^2 a}{2\varepsilon^2}\right), \tag{10a}$$

$$a'' - \bar{k}_y^2 a - a = \kappa s. \tag{10b}$$

In contrast to Eqs. (9), the coefficients in Eqs. (10) are independent of ξ and so Eqs. (10) can be Fourier transformed in the ξ direction, i.e., we may replace $d/d\xi \to i\bar{k}_x$ with $\bar{k}_x = k_x c/\omega_{pe}$. Defining $k = \sqrt{k_x^2 + k_y^2}$ and $\cos\theta = \mathrm{k}\cdot\mathrm{B}/(kB) = k_y/k$ gives $\bar{k}_y = (kc/\omega_{pe})\cos\theta$. Then, if we define $\gamma = -i\omega$, the determinant of Eqs. (10) is precisely the whistler dispersion relation with finite electron inertia included,[41] namely,

$$\frac{k^2c^2}{\omega^2} = \frac{\omega_{pe}^2}{\omega(|\omega_{ce}|\cos\theta - \omega)}. \tag{11}$$

Thus, Eqs. (9) generalize the uniform plasma equations giving the finite-electron-inertia whistler wave to the situation of a highly non-uniform magnetic field with associated current sheet. In this non-uniform situation, various coefficients in Eqs. (9) depend on ξ so the replacement $d/d\xi \to i\bar{k}_x$ is forbidden. Equations (9) must therefore be solved as coupled differential equations with non-constant coefficients; the method for this solution will be presented in Sec. III below. The definition of the reference frequency ω_{wh} corresponds to the frequency obtained from Eq. (11) in the limit $|\omega_{ce}|\cos\theta \gg \omega$ and $k \approx k_x \approx L^{-1} \gg k_y$; this reference frequency should be understood to be a frequency that scales like a whistler wave frequency, yet is not the frequency of any actual whistler wave.

III. SOLUTIONS WITH EIGENVALUE SATISFYING BOUNDARY CONDITIONS OF COUPLED EQUATIONS

If $\kappa \to 0$, no physically sensible unstable solution of Eqs. (9) exists because s and a are everywhere concave (i.e., $s''/s > 0$, $a''/a > 0$) and so diverge as $|\xi| \to \infty$. When $\xi \to 0$, the solutions are concave for any value of κ because the right hand sides of Eqs. (9) vanish. However, if for some critical κ there exist finite positive and negative ranges of ξ where the solutions are convex (i.e., $s''/s < 0$, $a''/a < 0$), the solutions in these convex regions can smoothly join the solution in the concave region centered about $\xi = 0$ to the exponentially decaying concave regions at $\xi \to \infty$ and $\xi \to -\infty$. Thus, like the bound-state solution of a localized potential well in a Schrödinger equation, the critical eigenvalue κ enables existence of a localized solution, i.e., a solution that is non-zero for finite ξ and yet vanishes as $|\xi| \to \infty$. The problem reduces to finding the eigenvalue κ that gives solutions which (1) vanish as $|\xi| \to \infty$, (2) satisfy $a(-\xi) = a(\xi)$, $s(-\xi) = -s(\xi)$, and (3) are smooth everywhere since the differential equations are smooth. The eigenvalue depends on all terms in Eqs. (9) and so cannot be estimated by making approximate solutions to selected sub-equations extracted from Eqs. (9).

If $\bar{k}_y^2$ and $\bar{\nu}_{ei}$ are assumed zero, solving Eqs. (9) numerically gives $\kappa = \kappa(\varepsilon)$ which then gives γ. Finite $\bar{\nu}_{ei}$ and finite $\bar{k}_y^2$ will modify this rate, but typically $\bar{k}_y^2$ can be assumed to be negligible for problems of interest (this corresponds to the reconnection layer being very thin). Equations (9) are solved numerically in an Interactive Data Language (IDL) code for κ using a two-point boundary value method[39] over the half-domain $0 \le \xi \le l_{\max}$ with $l_{\max} \gg 1$ to approximate $\xi = +\infty$. The critical value of κ is found by adjusting its value to satisfy a symmetry condition required when the half-domain is mapped to the full domain. The two-point boundary conditions are prescribed on the half-domain $0 \le \xi \le l_{\max}$ as

$$a(0) = -1, \quad a(l_{\max}) = 0, \tag{12a}$$

$$s(0) = 0, \quad s(l_{\max}) = 0; \tag{12b}$$

these boundary conditions satisfy the requirements that a and s vanish at $\xi = +\infty$ and that s is an odd function of ξ. A solution to Eqs. (9) can always be found for these boundary conditions for any κ. Because of the boundary condition at $\xi = l_{\max}$, the solution is guaranteed to decay at large ξ. Negative polarity is chosen for $a(0)$ to make $\tilde{E}_z J_z \sim -\gamma a J_z$ positive; this corresponds to the exponentially growing perturbation acting as a sink for electromagnetic energy.

The solution obtained for the half-domain $0 \le \xi \le l_{\max}$ is then used to construct a solution for the desired full domain $-l_{\max} \le \xi \le l_{\max}$ by defining $a(-\xi) = a(\xi)$ and defining $s(-\xi) = -s(\xi)$. Since $s(0) = 0$ was prescribed, this definition of s for negative ξ gives a smooth, continuous odd function $s(\xi)$. However, for an arbitrarily chosen κ, in general a' is finite at $\xi = 0$ in which case setting $a(-\xi) = a(\xi)$, i.e., mirroring $a(\xi)$ about $\xi = 0$, produces a discontinuity in a'. Because Eq. (9) has finite a'' at $\xi = 0$, such a discontinuity in a' is impermissible. Thus, to find a permissible solution (i.e., a smooth solution), κ is adjusted until a value is found for which a' vanishes at $\xi = 0$. For this choice of κ, we may let $a(-\xi) = a(\xi)$ and $s(-\xi) = -s(\xi)$ to obtain solutions in the full $-l_{\max} \le \xi \le l_{\max}$ domain; these solutions have no discontinuities since mirroring of $a' = 0$ still gives $a' = 0$. A value of κ that gives $a' = 0$ at $\xi = 0$ is thus an eigenvalue for the problem.

There is a discrete spectrum of κ eigenvalues, much like the discrete spectrum of eigenvalues for the bound states of a Schrödinger equation. The smallest κ corresponds to the

fastest growth rate (largest γ) and least amount of spatial oscillation in $a(\xi)$ and $s(\xi)$. In considering reconnection, we are only interested in the smallest κ eigenvalue since its associated eigenfunction grows fastest and will quickly dominate all others.

In order to find the smallest κ eigenvalue, a function $D(\kappa)$ is defined as $D(\kappa)=a'(0)$. The numerical positive ξ domain consists of N grid points $\{0, \Delta, 2\Delta, 3\Delta, \ldots (N-1)\Delta\}$ where $\Delta = l_{\max}/(N-1)$ and so the numerical representation of the derivative of $a(\xi)$ at $\xi=0$ is $a'(0)=(a(\Delta)-a(0))/\Delta$. Numerical solutions of Eqs. (9) were obtained using $N=500$ and $l_{\max}=40$; these define Δ while Eq. (12a) prescribes $a(0)$ so all that is needed to determine $D(\kappa)$ is $a(\Delta)$. For a given κ, the numerical solution to Eqs. (9) gives $a(\Delta)$ and so with this $D(\kappa)=(a(\Delta)-a(0))/\Delta$ is fully determined. The iterative root-finding procedure FX_ROOT in the IDL language is then used to find the root κ of $D(\kappa)=0$; FX_ROOT uses Muller's method as described in Ref. 42. Inspection of Eqs. (9) shows that κ cannot be arbitrarily small because if this were to happen, the right hand side of Eqs. (9) would also be arbitrarily small in which case a and s would become concave everywhere and so violate the boundary condition that a and s are finite as $|\xi| \to \infty$.

This smallest κ for which $a'(0)=0$ corresponds to the largest γ, i.e., the fastest growing mode. Figure 2 plots the $a(\xi)$ and $s(\xi)$ numerical solutions as black solid and red dashed lines, respectively, for a sequence of ε values and for $\bar{\nu}_{ei}=0$. For reference, $\tanh(\varepsilon\xi)$ is plotted as a blue dotted line. The value of κ determined by the root-finding procedure is listed in each ε plot. Figure 3 shows similar plots except now $\bar{\nu}_{ei}=2$; this shows that finite resistivity broadens the $s(\xi)$ profile, has little effect on the $a(\xi)$ profile, and moderately increases the growth rate at small ε. These plots have been normalized so that the maximum magnitude of $a(\xi)$ is always unity. In these plots $\bar{k}_y$ has been assumed to be zero. It is seen that $a(\xi)$ is negative for all ξ so $\tilde{E}_z J_z > 0$ everywhere. This means that the instability feeds off the initial stored magnetic energy (i.e., dissipates the initial magnetic energy) and also that the sign of $\hat{x}\cdot\tilde{\mathbf{E}}\times\mathbf{B}=-\tilde{E}_z B_y$ corresponds to fluid inflow towards the X-point in the vicinity of the $y=0$ axis.

IV. COMPARISON TO MRX

Using the MRX parameters[25,40] of $c/\omega_{pe}=0.15$ cm, $L=2$ cm, $\omega_{ce}/2\pi=300$ MHz, $\omega_{pe}/2\pi=30$ GHz gives $\varepsilon\approx 0.08$ and $v_{Ae}=c\omega_{ce}/\omega_{pe}\approx 3\times10^6$ m/s. The distance from the symmetry line to the local maximum of the quadrupole magnetic field is $l_y\simeq 6$ cm so $k_y=\pi/(2l_y)\simeq 25\,\mathrm{m}^{-1}$. Thus, $\omega_{wh}=k_y\varepsilon v_{Ae}\approx 6\times10^6\,\mathrm{s}^{-1}$. Using $\nu_{ei}\approx 2\times10^7$ gives $\bar{\nu}_{ei}\approx 2$. For these values of ε and $\bar{\nu}_{ei}$, the bottom-most numerical solution in Fig. 3 gives $\kappa\simeq 7$ corresponding to a linear growth rate $\gamma=\sqrt{2}\omega_{wh}/\kappa\approx 10^6\ \mathrm{s}^{-1}$ which is sufficiently fast for the configuration to reach a saturated state in the 4 μs characteristic time of the experiment. If this were not the case, reconnection could not occur within 4 μs because linear instability necessarily precedes nonlinear saturation.

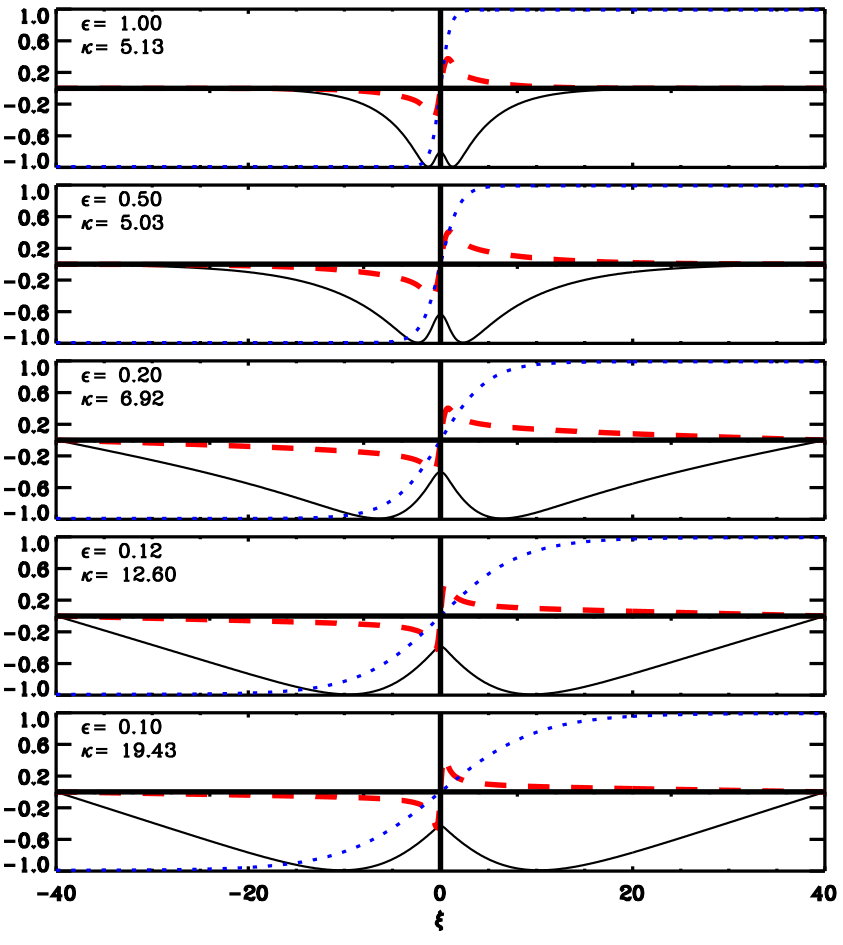

FIG. 2. Numerically calculated solutions to Eqs. (9) for $\bar{\nu}_{ei}=0$ and $\bar{k}_y=0$ and a range of ε values with κ selected to be the smallest value that gives $a'=0$ at $\xi=0$. The function $a(\xi)$ is shown as a heavy black solid line and the function $s(\xi)$ is shown as a heavy dashed red line; $\tanh(\varepsilon\xi)$ is shown for reference as a light dotted blue line.

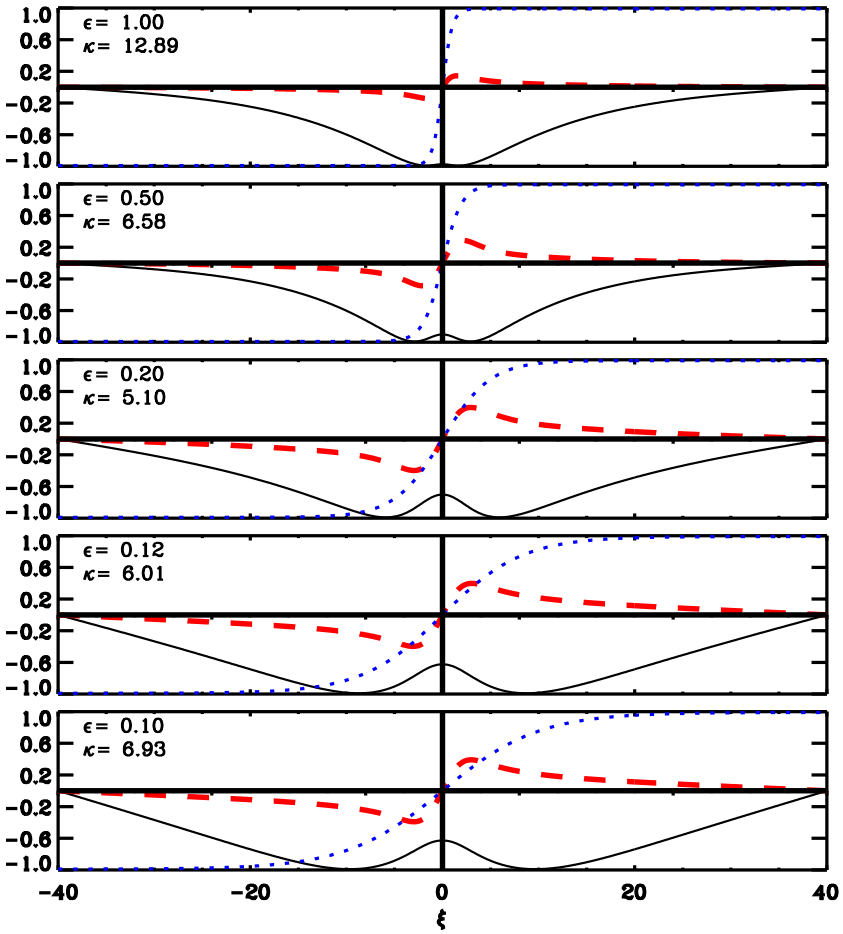

FIG. 3. Same as Fig. 2, except $\bar{\nu}_{ei} = 2$.

Because ω_{wh} is independent of electron mass and because κ is of order 5–10 for a large range of ε, the growth rate γ is only weakly dependent on electron inertia. Although only weakly affecting γ, electron inertia is nevertheless important because it determines the reconnection region spatial scale; this conclusion is consistent with observations reported in Refs. 25 and 26 where it was found that the steady-state reconnection rate does not depend significantly on resistivity or on electron inertia but the reconnection region spans a few electron inertia scale lengths.

The reason for this weak dependence of growth rate on electron inertia and resistivity can be seen from inspection of Eqs. (9). Because of the ε^2 in the denominator in the right hand side of Eq. (9a) and assuming $s \ll a$ and $\kappa \gg 1$ it is seen that a is approximately determined by setting the right hand side of Eq. (9a) to zero. Assuming $\tanh^2(\varepsilon\xi) \approx 1/2$ (i.e., $\xi \simeq 0.9/\varepsilon$) as a nominal value, it is seen that a approximately satisfies $a'' + \varepsilon^2 a = 0$. Near its peak $a \sim \cos(\varepsilon\xi)$ so a has a characteristic scale $\sim 1/\varepsilon$ which is confirmed by examination of how the $a(\xi)$ plots in Figs. 2 and 3 scale with ε. Since $a'' \approx -\varepsilon^2 a$ the term involving resistivity (i.e., term with $\bar{\nu}_{ei}$) on the left hand side of Eq. (9b) is small relative to the a term; because $\kappa \gg 1$, the remainder of Eq. (9b) shows that $s \approx -\kappa^{-1} a$ and so $|s| \ll |a|$ as was assumed. Since Eq. (9b) is just a rescaled form of Eq. (4a), it is seen that ηJ_z is small compared to the other terms in Eq. (4a) if ξ is sufficiently far from zero so that s is finite; from Fig. 3 it is seen that this corresponds to $2 < |\xi| < 10$. This requirement for ξ to be finite is because the hyperbolic symmetry of A_z and the quadrupolar nature of B_z necessitate that $\mathbf{B}_T$ and $\mathbf{J}_T$, respectively, vanish exactly on the X-point, i.e., symmetry implies $\hat{z} \cdot \mathbf{J}_T \times \mathbf{B}_T = 0$ exactly on the X-point. While finite resistivity makes ηJ_z dominate the finite electron inertia term $\sim \partial J_z/\partial t$ in Eq. (4a) (i.e., $\bar{\nu}_{ei}$ exceeds unity), this has little consequence because the finite electron inertia term itself is relatively unimportant in Eq. (4a). On the other hand, finite electron inertia is what provides $\varepsilon \ll 1$ and it is this scaling that necessitates setting the right hand side of Eq. (9a) to zero to solve the coupled equations if $2 < |\xi| < 10$. Since the term corresponding to $\eta\tilde{J}_z$ in Eq. (9b) is $\kappa\bar{\nu}_{ei}a''$ and the term in Eq. (9b) corresponding to $\tilde{E}_z$ is a, the ratio $\eta\tilde{J}_z/\tilde{E}_z \approx \kappa\bar{\nu}_{ei}a''/a \approx \kappa\bar{\nu}_{ei}\varepsilon^2 \simeq 0.14$. The mapping of MRX coordinates $\{R, Z, T\}$ to the Cartesian coordinates used here is $\{R, Z, T\} \leftrightarrow \{x, y, z\}$ so this ratio is in reasonable agreement with the experimental measurement in Ref. 25 where it was observed that $\eta J_T/E_T = (40\,\text{V/m})/(170\,\text{V/m}) = 0.25$ if it is assumed that the measurement location was at least a few skin depths from the X-point so $\hat{z} \cdot \mathbf{J}_T \times \mathbf{B}_T \neq 0$.

Figures 2 and 3 also provide a means for making an approximate quantitative comparison to MRX v_{eZ} measurements[25] (i.e., electron outflow corresponding to $-\tilde{J}_y/ne$ here). In particular, the plots in Figs. 2 and 3 show that s has a minimum to the left of the ξ origin and a maximum to the right. Since $\tilde{J}_y = -\mu_0^{-1}\partial B_z/\partial x \sim ds/d\xi$, it is seen that $\tilde{J}_y$ reverses polarity when $ds/d\xi$ vanishes, i.e., at the extrema of s. The separation between the left and right locations where $\tilde{J}_y$ changes polarity is thus the distance between the maxima and minima of s in Figs. 2 and 3. For the $\varepsilon = 0.1$ plot in Fig. 3, this

separation is about 8 electron skin depths, i.e., about 1.2 cm. Ren *et al.*[25] plot $v_{eZ}(R)$ in their Fig. 2(b) where it is seen that the zero crossings (vertical dashed line locations) are separated by 3.3 cm which is a factor of 3 larger than the 1.2 cm prediction of the $\varepsilon = 0.1$ plot in Fig. 3. This discrepancy of $\sim 3\times$ wider observed than predicted electron outflow has also been seen when comparing Particle-in-Cell (PIC) simulations to the MRX measurements as discussed by Ji *et al.*[43]

V. COMPARISON TO ROGERS *ET AL.*

We first show that the two-fluid analysis used by Rogers *et al.* (Eqs. (1) and (2) of Ref. 28) to explain their numerical simulation results corresponds to keeping only the right hand sides of Eqs. (4a) and (5) in which case Eqs. (4a) and (5) reduce to

$$E_z - \frac{1}{ne}\hat{z}\cdot \mathbf{J}_T \times \mathbf{B}_T = 0, \tag{13a}$$

$$\frac{\partial B_z}{\partial t} + \frac{1}{ne}\hat{z}\cdot \nabla_T \times (\mathbf{J}\times \mathbf{B})_T = 0. \tag{13b}$$

Using $E_z = -\partial A_z/\partial t, \nabla_T = \nabla, \mathbf{B}_T = \nabla A_z \times \hat{z}, \mathbf{J}_T = \mu_0^{-1}\nabla_T B_z \times \hat{z}$ and $J_z = -\mu_0^{-1}\nabla_T^2 A_z$, Eqs. (13) become Eqs. (1) and (2) of Ref. 28. The omission of the left hand sides of Eqs. (4a) and (5) (i.e., omitting finite electron inertia and finite resistivity) corresponds to omitting the terms containing the factors $(1+\kappa\bar{\nu}_{ei})$ on the left hand sides of Eqs. (9a) and (9b). Thus, Eqs. (1) and (2) of Ref. 28 are equivalent to

$$-s = \kappa\left(\frac{a'' - \bar{k}_y^2 a}{2\varepsilon^2} + a\left(1-\tanh^2(\varepsilon\xi)\right)\right)\tanh(\varepsilon\xi), \tag{14a}$$

$$-a = \kappa s \tanh(\varepsilon\xi). \tag{14b}$$

Substituting for s in Eq. (14a) using Eq. (14b) gives the *second-order* differential equation

$$a''\tanh^2(\varepsilon\xi) - \left[\bar{k}_y^2\tanh^2(\varepsilon\xi) + 2\varepsilon^2\tanh^2\varepsilon\xi \times \left(1-\tanh^2(\varepsilon\xi)\right) - 2\frac{\varepsilon^2}{\kappa^2}\right]a = 0, \tag{15}$$

which in the vicinity of $\xi = 0$ reduces to

$$\xi^2 a'' + \frac{2}{\kappa^2}a = 0. \tag{16}$$

The two solutions to Eq. (16) are

$$a_\pm = \xi^{p\pm}, \tag{17}$$

where

$$p_\pm = \frac{1}{2} \pm \sqrt{\frac{1}{4} - \frac{2}{\kappa^2}}. \tag{18}$$

Because $p_\pm$ is neither zero nor a positive integer, derivatives of $a_\pm$ are singular at $\xi = 0$ and so the solutions given by Eq. (17) are non-physical. In particular, because $\tilde{J}_z \sim -\partial^2\tilde{A}_z/\partial x^2 \sim -a''$ it is seen that Eq. (15) gives the non-physical prediction that $\tilde{J}_z$ would be infinite at $x = 0$. Thus, while a mathematical solution exists at $x = 0$, this mathematical solution is not regular and so not physically allowable.[44] In order to have physically sensible solutions, it is therefore necessary to retain at least one of finite electron mass or finite collisionality and use the fourth-order system of equations given by the coupled Eqs. (9a) and (9b).

Equation (14b) is just Eq. (4) of Rogers *et al.*[28] expressed in the variables defined by Eqs. (6) and (7). Rogers *et al.* pointed out that the out-of-plane magnetic field is the stream function for the in-plane electron flows and then stated that according to their Eq. (2) these flows are frozen into the in-plane magnetic field. However, we have just shown here that Eq. (14b) which corresponds to Eq. (2) of Rogers *et al.* is missing the term $(1+\kappa\bar{\nu}_{ei})$ $(a''$ - $\bar{k}_y^2 a)$ that appears in the left hand side of Eq. (9b). We have also shown that this missing term comes from inclusion of finite electron inertia (the "1" in parenthesis) and from finite resistivity (the $\kappa\bar{\nu}_{ei}$ term in parenthesis). Thus, the in-plane magnetic field is not frozen to the in-plane electron flows when $(1+\kappa\bar{\nu}_{ei})$ $(a'' - \bar{k}_y^2 a)$ is kept in Eq. (9b). Since the finiteness of $(1+\kappa\bar{\nu}_{ei})$ $(a'' - \bar{k}_y^2 a)$ is what distinguishes the fourth-order solutions from the second-order solutions near $\xi = 0$, inclusion of finite electron inertia or finite resistivity near $\xi = 0$ unfreezes the in-plane magnetic field from the in-plane electron flows.

It should also be noted that the simple standing whistler wave model proposed in Rogers *et al.* leads to non-physical behavior as follows: Rogers *et al.* postulated that the whistler wave wavenumber should be modeled as $k \sim \pi/y$ in the vicinity of the X-point and that reconnection would involve electron outflows having a standing wave dependence $\sim \cos(kx)\sin(\omega t)$. Such a dependence is non-physical as it predicts that the direction of the electron flow rapidly oscillates at the high frequency ω so the "outflow" rapidly alternates between being an outflow and an inflow; furthermore, this oscillation occurs with a non-physical infinite frequency at $y = 0$ since $k \sim \pi/y$ and $\omega \sim k^2$ were assumed.

VI. COMPARISON TO MANDT *ET AL.*

Mandt *et al.*[27] used hybrid simulations to examine the merging of two flux bundles (i.e., mutually attracting parallel currents) where the initial mutual attraction was balanced by electron pressure resulting from spatially non-uniform electron temperature (density and ion temperature were considered uniform). Because the system started in force balance (equilibrium), there would presumably have to be an imposed perturbation since otherwise the system would stay in force balance indefinitely. They conducted simulations for different values of L where L was measured in units of ion skin depth c/ω_{pi} and L was the characteristic dimension of a flux bundle. The total reconnection time τ measured in units of ω_{ci}^{-1} was plotted for various L values for two η values and also for a case where the ion equation of motion was not evolved. Linear instability of the initial equilibrium necessarily precedes nonlinear saturation. Although the amplitude of the initial perturbation was not stated in Ref. 27, it presumably was not infinitesimal because if so, the time to reach nonlinear saturation would become arbitrarily long. If the

initial perturbation was not infinitesimal and yet small compared to unity, a value of 10% would seem reasonable (this has been typically been used in other numerical simulations). A 10% initial perturbation would become an 80% perturbation after $t=2\gamma^{-1}$ at which time the system would be close to nonlinear saturation. Thus, it is reasonable to assume that the "total reconnection time" given in Fig. 2 of Ref. 27 would be a few times γ^{-1} and so would have approximately the same logarithm as γ^{-1}.

Because Mandt *et al*. have their flux bundle scale with L, they effectively had both the x and y components scale with L so the shape of the bundle remained the same. Hence, in order to compare their simulation results with our results, k_y in our system must be made to scale as L^{-1} in order to have the bundle shape remain the same when L is changed. We recall now our result that κ is a weak function of ε. In particular, we found that, within a factor of two accuracy, our results give $\kappa \simeq 10$ for a wide range of ε (recall that κ varies from $\sim$6 to $\sim$18 as ε ranges from 0.1 to 1). Using this $\kappa \simeq 10$ result, our calculation predicts that a self-similar collisionless or weakly resistive situation will have a growth rate

$$\gamma \approx \frac{2^{1/2}}{10L^2}\frac{\bar{B}}{ne\mu_0}. \tag{19}$$

Upon dividing both sides by $\omega_{ci}=e\bar{B}/m_i$ and then inverting both sides this becomes

$$\frac{\omega_{ci}}{\gamma} \approx \frac{10}{2^{1/2}}\left(\frac{L}{c/\omega_{pi}}\right)^2. \tag{20}$$

Taking the logarithm to base 10 of both sides gives

$$\log_{10}\left(\gamma^{-1}\omega_{ci}\right) = 2\log_{10}\left(\frac{L}{c/\omega_{pi}}\right) + \log_{10}\left(\frac{10}{2^{1/2}}\right). \tag{21}$$

Defining $\tau=\gamma^{-1}\omega_{ci}$ to be the nominal reconnection time measured in units of ω_{ci}^{-1}, it is seen the slope of a log-log plot of τ versus L measured in terms of ion skin depths should be 2. This prediction is in good agreement with the line through the triangle points in Fig. 2 of Mandt *et al*. which has a slope of 2 since a two-decade change in L gives a 4-decade change in τ. The triangle points in Fig. 2 of Mandt *et al*. are for a situation where there is no ion motion and $L<c/\omega_{pi}$. Setting $k_y=L^{-1}$ has an about a factor of 2 ambiguity and the shape given in Fig. 1 of Mandt *et al*. is not a precise cosine. However, these issues are of order unity and so are not significant when taking the logarithm. Evaluation of the offset in Eq. (21) gives $\log_{10}(10/2^{1/2})=0.8$ which implies that we predict $\log_{10}(\gamma^{-1}\omega_{ci})=0.8$ when $L/(c/\omega_{pi})=1$. Examination of the triangles plotted in Fig. 2 of Mandt *et al*. shows that the line through these triangles is in excellent agreement with our prediction. It should be noted that dividing both sides of Eq. (19) by ω_{ci} introduced an apparent dependence on ion inertia. No such dependence actually exists because Eq. (19) had no inertia. We could just as easily have divided both sides by ω_{ce} and obtained a completely equivalent form of Eq. (21) where $\omega_{ci}\rightarrow\omega_{ce}$ and $\omega_{pi}\rightarrow\omega_{pe}$; this is because $\omega_{pi}^2/\omega_{ci}=\omega_{pe}^2/|\omega_{ce}|=c^2ne\mu_0/B$ contains no inertia.

VII. CONCLUSIONS

The resistive MHD description of magnetic reconnection involves a system of equations having no involvement of B_z and so is a second order differential equation in x with a diffusive inner region. In contrast, here the system of equations is inherently fourth-order, involves two variables (i.e., A_z and B_z), and is not diffusive. This shows that incorporating the Hall and finite electron inertia terms does not produce a mere correction to the MHD description, but rather produces a completely different sort of dynamics. Omission of both finite electron mass and collisions from the two-fluid equations leads to a second- rather than fourth-order system of differential equations; the solution of this second-order system is physically defective because it predicts an infinite current density at $x=0$.

ACKNOWLEDGMENTS

This material is based upon work supported by the U.S. Department of Energy Office of Science, Office of Fusion Energy Sciences under Award Nos. DE-FG02-04ER54755 and DE-SC0010471, by the National Science Foundation under Award No. 1059519, and by the Air Force Office of Scientific Research under Award No. FA9550-11-1-0184.

[1]E. Priest and T. Forbes, *Magnetic Reconnection* (Cambridge University Press, Cambridge, 2000).
[2]E. G. Zweibel and M. Yamada, in Annual Review of Astronomy and Astrophysics, edited by R. Blandford, J. Kormendy, and E. VanDishoeck (2009), Vol. 47, pp. 291–332.
[3]M. Yamada, R. Kulsrud, and H. T. Ji, Rev. Mod. Phys. **82**, 603 (2010).
[4]H. Karimabadi, V. Roytershteyn, W. Daughton, and Y. H. Liu, Space Sci. Rev. **178**, 307 (2013).
[5]Y. Ono, M. Inomoto, T. Okazaki, and Y. Ueda, Phys. Plasmas **4**, 1953 (1997).
[6]M. R. Brown, Phys. Plasmas **6**, 1717 (1999).
[7]M. Yamada, H. T. Ji, S. Hsu, T. Carter, R. Kulsrud, and F. Trintchouk, Phys. Plasmas **7**, 1781 (2000).
[8]M. Yamada, Y. Ren, H. Ji, J. Breslau, S. Gerhardt, R. Kulsrud, and A. Kuritsyn, Phys. Plasmas **13**, 052119 (2006).
[9]X. H. Deng and H. Matsumoto, Nature **410**, 557 (2001).
[10]M. Oieroset, T. D. Phan, M. Fujimoto, R. P. Lin, and R. P. Lepping, Nature **412**, 414 (2001).
[11]S. Masuda, T. Kosugi, H. Hara, and Y. Ogawara, Nature **371**, 495 (1994).
[12]M. J. Aschwanden, Space Sci. Rev. **101**, 1 (2002).
[13]B. Zhang and H. R. Yan, Astrophys. J. **726**, 90 (2011).
[14]P. Helander, L. G. Eriksson, and F. Andersson, Plasma Phys. Controlled Fusion **44**, B247 (2002).
[15]M. R. Brown, C. D. Cothran, M. Landreman, D. Schlossberg, W. H. Matthaeus, G. Qin, V. S. Lukin, and T. Gray, Phys. Plasmas **9**, 2077 (2002).
[16]D. Biskamp, *Magnetic Reconnection in Plasmas* (Cambridge University Press, Cambridge, 2000).
[17]P. A. Sweet, *The Neutral Point Theory of Solar Flares* (Cambridge Univ. Press, 1958), Vol. 6 of IAU Symposia, p. 123.
[18]E. N. Parker, J. Geophys. Res. **62**, 509, doi:10.1029/JZ062i004p00509 (1957).
[19]H. P. Furth, J. Killeen, and M. N. Rosenbluth, Phys. Fluids **6**, 459 (1963).
[20]B. Coppi, G. Laval, and R. Pellat, Phys. Rev. Lett. **16**, 1207 (1966).
[21]L. Spitzer, *Physics of Fully Ionized Gases* (Interscience, New York, 1956), p. 21, Eqs.(2)–(12).
[22]A. Runov, R. Nakamura, W. Baumjohann, R. A. Treumann, T. L. Zhang, M. Volwerk, Z. Voros, A. Balogh, K. H. Glassmeier, B. Klecker *et al*., Geophys. Res. Lett. **30**, 1579, doi:10.1029/2002GL016730 (2003).
[23]C. D. Cothran, M. Landreman, M. R. Brown, and W. H. Matthaeus, Geophys. Res. Lett. **32**, L03105, doi:10.1029/2004GL021245 (2005).
[24]M. R. Brown, C. D. Cothran, and J. Fung, Phys. Plasmas **13**, 056503 (2006).

[25]Y. Ren, M. Yamada, H. Ji, S. P. Gerhardt, and R. Kulsrud, Phys. Rev. Lett. **101**, 085003 (2008).
[26]Y. Ren, M. Yamada, H. Ji, S. Dorfman, S. P. Gerhardt, and R. Kulsrud, Phys. Plasmas **15**, 082113 (2008).
[27]M. E. Mandt, R. E. Denton, and J. F. Drake, Geophys. Res. Lett. **21**, 73, doi:10.1029/93GL03382 (1994).
[28]B. N. Rogers, R. E. Denton, J. F. Drake, and M. A. Shay, Phys. Rev. Lett. **87**, 195004 (2001).
[29]J. Birn, J. F. Drake, M. A. Shay, B. N. Rogers, R. E. Denton, M. Hesse, M. Kuznetsova, Z. W. Ma, A. Bhattacharjee, A. Otto *et al*., J. Geophys. Res.: Space Phys. **106**, 3715 (2001).
[30]P. A. Cassak, M. A. Shay, and J. F. Drake, Phys. Rev. Lett. **95**, 235002 (2005).
[31]E. G. Harris, Nuovo Cimento **23**, 115 (1962).
[32]P. L. Pritchett, J. Geophy. Res.: Space Phys. **106**, 3783 (2001).
[33]B. Sonnerup, in *Solar System Plasma Processes*, edited by L. Lanzerotti, C. Kennel, and E. Parker (North-Holland, Washington, 1979), Vol. 3, p. 45.
[34]K. Fujimoto and R. D. Sydora, Geophys. Res. Lett. **35**, L19112, doi:10.1029/2008GL035201 (2008).
[35]J. Guo, B. Yu, G. H. Guo, and B. Zhao, Chin. Phys. Lett. **28**, 025201 (2011).
[36]S. V. Bulanov, F. Pegoraro, and A. S. Sakharov, Phys. Fluids B **4**, 2499 (1992).
[37]N. Attico, F. Califano, and F. Pegoraro, Phys. Plasmas **7**, 2381 (2000).
[38]I. F. Shaikhislamov, J. Plasma Phys. **74**, 215 (2008).
[39]P. M. Bellan, J. Comput. Phys. **136**, 654 (1997).
[40]J. Yoo, Ph.D. dissertation, Princeton University, 2013.
[41]T. H. Stix, *Waves in Plasmas* (American Institute of Physics Press, New York, 1992).
[42]W. H. Press, B. P. Flannery, S. A. Teukolsky, and W. T. Vetterling, *Numerical Recipes* (Cambridge University Press, Cambridge, 1986), Sec. 9.5, p. 262.
[43]H. Ji, Y. Ren, M. Yamada, S. Dorfman, W. Daughton, and S. P. Gerhardt, Geophys. Res. Lett. **35**, L13106, doi:10.1029/2008GL034538 (2008).
[44]H. R. Lewis and P. M. Bellan, J. Math. Phys. **31**, 2592 (1990).